Dalton Transactions



PAPER View Article Online View Journal



Cite this: DOI: 10.1039/d1dt02175c

Electrocatalytic nitrate reduction with Co-based catalysts: comparison of DIM, TIM and cyclam ligands†

Hyuk-Yong Kwon, Da Sarah E. Braley, Jose P. Madriaga, D‡c Jeremy M. Smith **D** and Elena Jakubikova **D***

Over the past century, the global concentration of environmental nitrate has increased significantly from human activity, which has resulted in the contamination of drinking water and aquatic hypoxia around the world, so the development of effective nitrate-reducing agents is urgent. This work compares three potential macrocycle-based nitrate reduction electrocatalysts: $[Co(DIM)]^{3+}$, $[Co(cyclam)]^{3+}$ and $[Co(TIM)]^{3+}$. Although all three complexes have similar structures, only $[Co(DIM)]^{3+}$ has been experimentally determined to be an active electrocatalyst for selective nitrate reduction to produce ammonia in water. While $[Co(cyclam)]^{3+}$ can reduce aqueous nitrate to ammonia and hydroxylamine at heavy metal electrodes, $[Co(TIM)]^{3+}$ is inactive for the reduction of nitrate. As an initial step to understanding what structural and electronic properties are important for efficient electrocatalysts for nitrate reduction, density functional theory (DFT) was employed to investigate the electronic structure of the three Co complexes, with the reduction potentials calibrated to experimental results. Moreover, DFT was employed to explore four different reaction mechanisms for the first steps of nitrate reduction. The calculated reaction barriers reveal how a combination of electron transfer in a redox non-innocent complex, substrate binding, and intramolecular hydrogen bonding dictates the activity of Co-based catalysts toward nitrate reduction.

Received 29th June 2021, Accepted 11th August 2021 DOI: 10.1039/d1dt02175c rsc.li/dalton

Introduction

Development of the Haber–Bosch process in the beginning of the 20th century allowed ammonia to be mass-produced for various applications such as fertilizers and explosives. Since then ammonia has become one of the most produced inorganic compounds; about 140 million metric tons of ammonia were produced in 2018. With the increased use of nitrogen fertilizers, people have benefitted from better productivity of agricultural crops. However, most nitrogen-based

fertilizers are not absorbed by crops; instead about 70 percent are lost to the environment. And a subsequent electrochemical nitrate causes serious diseases when consumed, such as blue baby syndrome, and promotes the growth of cyanobacteria, which results in aquatic hypoxia. Nitrate capture, and subsequent electrochemical nitrate reduction to useful chemicals such as ammonia, presents one potential pathway to alleviating the environmental impact of excess nitrate.

Several previous studies showed that Co complexes can electrocatalytically reduce nitrogen oxides in aqueous solution. A cobalt tetrakis(*N*-methyl-2-pyridyl)porphine (Co(2-TMPyP)) was determined to reduce nitrite and nitric oxide to yield ammonia and hydroxylamine. Additionally, a cobalt-tripeptide complex (CoGGH) was recently determined to be an efficient catalyst for nitrite reduction. However, there are only few reported Co catalysts that can reduce nitrate. [Co(DIM)]³⁺ (DIM = 2,3-dimethyl-1,4,8,11-tetraazacyclotetradeca-1,3-diene, see Fig. 1) was found to be a selective electrocatalyst for nitrate reduction to yield ammonia, albeit at large overpo-

^aDepartment of Chemistry, North Carolina State University, 2620 Yarbrough Dr., Raleigh, NC 27695, USA. E-mail: ejakubi@ncsu.edu

^bDepartment of Chemistry, Indiana University, 800 E. Kirkwood Ave., Bloomington, IN 47401, USA. E-mail: smith962@indiana.edu

^cDepartment of Chemistry, California Polytechnic University, San Luis Obispo, CA 93407, USA

[†] Electronic supplementary information (ESI) available: Experimental details; additional cyclic voltammetry data; additional discussion on investigated reaction mechanisms; additional discussion on the method dependence of calculated energetics; raw calculated energies for all species considered. Cartesian coordinates of optimized structures in their lowest energy spin states. See DOI: 10.1039/d1dt02175c

[‡]Current address: Department of Chemistry, Virginia Tech, Blacksburg, VA 24061, USA.

Paper **Dalton Transactions**

Fig. 1 Investigated tetradentate ligands: cyclam, DIM and TIM.

tential.¹¹ Also, [Co(cyclam)]³⁺ (cyclam = 1,4,8,11-tetraazacyclotetradecane) is reported to produce hydroxylamine and ammonia under various conditions. 12-14

While [Co(cyclam)]3+ and [Co(DIM)]3+ were determined to be nitrate reducing electrocatalysts, [Co(TIM)]³⁺ (TIM = 2,4,9,10-tetramethyl-1,4,8,11-tetraazacyclodec-1,3,8,10-tetraene) did not show significant catalytic activity with nitrate despite the structural similarities of the three ligands. 15 The major structural differences between the investigated tetradentate ligands are (1) the number of the π -conjugated diimine groups and (2) the number of amino-protons. The absence of aminoprotons at the diimine portion of the macrocycle reduces the energetic penalties of conformational changes between square planar, square pyramidal, and seesaw conformations. On the other hand, through hydrogen bonding, the amino-protons can introduce nitrate or other substrates to the metal binding site and allow them to bind more tightly.

In this work, we employ density functional theory (DFT) along with electrochemical analysis to investigate the electronic structure of [Co(cyclam)]³⁺, [Co(DIM)]³⁺ and [Co(TIM)]³⁺ and the ability of each of these species to act as a nitrate reduction catalyst. Four mechanisms for nitrate reduction were investigated (shown in Fig. 2): monodentate, bidentate, hydroxyl transfer, and amino-proton-assisted mechanism. The monodentate, bidentate, and hydroxyl transfer mechanisms were investigated previously for nitrate reduction by a [Co (DIM)]3+ complex by Xu et al. 15 This work focuses on comparing the effectiveness of the three Co complexes as catalysts for nitrate reduction and identifies the amino-proton-assisted

Bidentate mechanism Hydroxyl transfer mechanism $\left[\begin{array}{ccc} \text{Co-L} \end{array} \right]^{+} \xrightarrow{+ \text{NO}_{3}^{-}} & \overset{\text{O}}{\overset{\text{N}}{\text{O}}} & \xrightarrow{+ \text{H}^{+}} & \left[\overset{\text{O}}{\overset{\text{N}}{\text{O}}} \overset{\text{O}}{\overset{\text{O}}{\text{O}}} \right]^{+} & \longrightarrow & \left[\overset{\text{N}}{\overset{\text{O}}{\text{O}}} \overset{\text{O}}{\overset{\text{O}}{\text{O}}} \right]^{+} \\ & \overset{\text{O}}{\overset{\text{O}}{\text{O}}} & \overset{\text{O}}{\overset{\text{O}}} & \overset{\text{O}}{\overset{\text{O}}{\text{O}}} & \overset{\text{O}}{\overset{\text{O}}{\text{O}}} & \overset{\text{O}}{\overset{\text{O}}{\text{O}}} & \overset{\text{O}}{\overset{\text{O}}{\text{O}}} & \overset{\text{O}}{\overset{\text{O}}{\text{O}}} & \overset{\text{O}}{\overset{\text{O}}} & \overset{\text{O}}{\overset{\text{O}}{\text{O}}} & \overset{\text{O}}{\overset{\text{O}}{\text{O}}} & \overset{\text{O}}{\overset{\text{O}}{\text{O}}} & \overset{\text{O}}{\overset{\text{O}}{\text{O}}} & \overset{\text{O}}{\overset{\text{O}}{\text{O}}} & \overset{\text{O}}{\overset{\text{O}}} & \overset{\text{O}}{\overset{\text{O}}{\text{O}}} & \overset{\text{O}}{\overset{\text{O}}{\text{O}}} & \overset{\text{O}}{\overset{\text{O}}{\text{O}}} & \overset{\text{O}}{\overset{\text{O}}{\text{O}}} & \overset{\text{O}}{\overset{\text{O}}} & \overset{\text{O}}{\overset{\text{O}}{\text{O}}} & \overset{\text{O}}{\overset{\text{O}}} & \overset{\text{$

Fig. 2 Investigated mechanisms for nitrate reduction.

mechanism as an additional feasible mechanism for nitrate reduction. The main objective is to discover the structural features that make the nitrate reduction process more favourable. In addition to providing insights into fundamental properties of small molecule catalysts, the understanding of these properties will provide future directions for designing better electrocatalysts.

Computational methodology

DFT calculations were performed using the Gaussian 16 software package Revision A.03 ¹⁶ employing the B3LYP¹⁷⁻²⁰ functional including Grimme's D2 dispersion correction²¹ (B3LYP+D2) and the implicit SMD model²² (with the exception of bromide ion where the default PCM model was used¹⁵) to account for solvent effects (water). An SDD pseudopotential (ECP10MDF) and accompanying basis set was used for Co.23,24 Br was also modelled with an SDD pseudopotential (ECP10MDF) and associated cc-pVTZ-PP basis set for geometry optimization and aug-cc-pVTZ-PP basis set for single point energy calculations.²⁵ For all other atoms, the 6-31G* basis set^{26,27} was used for geometry optimizations and frequency calculations, and then the electronic energies were determined from single point energy calculations performed on these geometries with 6-311+G** basis set. 28,29 An ultrafine grid was used for all calculations. The stability tests were performed for every complex to verify that the calculated wavefunction is the lowest energy electronic state. The free energy for each computed structure was obtained by adding the thermochemical corrections (at 298.15 K and 1.0 atm) to the single point energy. The final solvated free energy (G_{sol}) of all species including H⁺ was then adjusted to be at the standard state concentration of 1 M, with the exception of water which was treated as 55.5 M, which resulted in ΔG reported at pH = 0.30

Calculated reduction potentials (E°) were determined relative to the saturated calomel electrode (SCE) through eqn (1):

$$E^{\circ}(\text{eV}) = -\frac{\Delta G_{\text{sol}}}{nF} - 4.52 \tag{1}$$

where ΔG_{sol} is the change in solvated free energy upon reduction, n is the number of electrons transferred, and F is Faraday's constant. The calculated potentials are referenced to SCE by subtracting the absolute reduction potential of NHE, 4.28 V,³¹ which was determined by the aqueous solvation free energy of the proton, 265.9 kcal mol⁻¹, and converting the value relative to SCE (0.2412 vs. NHE). Note that when the DFT calculated reduction potentials of CoL2+ are compared with the onset potentials from cyclic voltammograms, the computational reduction potentials for $[Co(cyclam)(NO_3)]^+$, $[Co(DIM)]^{2+}$ and $[Co(TIM)]^{2+}$ complexes are more negative by approximately 0.3 V, which is consistent with previously published using studies the same computational methodology. 15,32

Dalton Transactions Paper

Results

Ground state electronic structure and spin-state energetics

While the ground states of all three investigated Co(III) (3d⁶) complexes are easy to analyse because they are closed-shell singlets, the DIM and TIM ligands in doubly-reduced Co(1) complexes become redox non-innocent. The two-electron reduced species [Co(DIM)]⁺ and [Co(TIM)]⁺ formally have Co(1) (3d⁸) electronic structures. However, the conjugated π^* orbitals of the diimine groups in DIM and TIM are similar in energy with Co 3d orbitals, which allows electrons from the Co(1) centre to be delocalized between the metal and the ligand. The natural orbitals in Fig. 3 show how the metal $3d_{yz}$ orbital and the ligand π^* orbital can interact to make bonding and antibonding pair combinations. As a result, four different spin states, antiferromagnetically-coupled singlet (AF-S), triplet (T), antiferromagnetically-coupled triplet (AF-T) and quintet (Q), are close in energy when this diimine group(s) is present (Table 1), especially when considering that the error range for DFT methods is ~5 kcal mol⁻¹.³³ Thus, all the spin states listed in Fig. 4 including singlet (S) were computed for every structure and the lowest energy spin state is listed for every structure in parentheses in Fig. 9-13.

Electrocatalytic activity of Co-macrocycle complexes

Aqueous cyclic voltammetry for $[Co(TIM)Br_2]^+$, $[Co(DIM)Br_2]^+$ and $[Co(cyclam)Br_2]^+$ was performed in the presence of 10 mM NaNO₃ (see Fig. 5). The measured onset potentials are approximately -0.6 V νs . SCE for TIM, -0.9 V νs . SCE for DIM and -1.3 V νs . SCE for cyclam. While the $[Co(cyclam)Br_2]^+$ and $[Co(DIM)Br_2]^+$ complexes showed irreversible catalytic waves, $[Co(DIM)Br_2]^+$

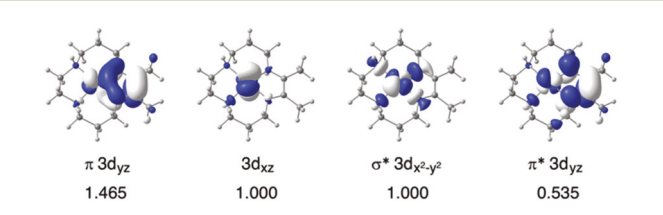


Fig. 3 Natural orbitals of [Co(DIM)]⁺ AF-T frontier orbitals with corresponding occupation numbers.

Table 1 Relative spin state energetics (ΔG) of each complex in kcal mol⁻¹. [Co(cyclam)]⁺ does not have stable antiferromagnetically-coupled states because there is no π conjugation in the ligand. Also, note that the closed shell singlets of [Co(DIM)]⁺ and [Co(TIM)]⁺ are electronically unstable

Spin state	[Co(cyclam)] ⁺	[Co(DIM)] ⁺	[Co(TIM)] ⁺	
S	5.7	_	_	
AF-S	_	1.4	0.7	
T	0.0	0.6	0.0	
AF-T	_	0.0	5.4	
Q	27.6	3.3	8.9	

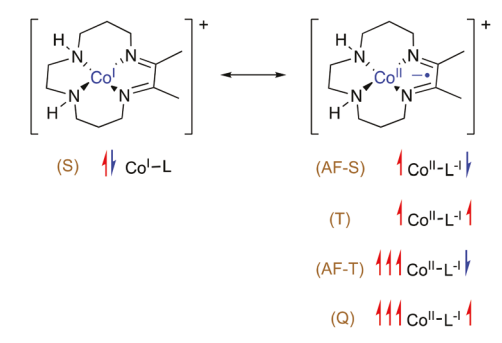


Fig. 4 Illustration of studied spin states for [Co(DIM)]⁺ organized by which "resonance structure" they resemble the most. [Co(TIM)]⁺ has similar spin state structures.

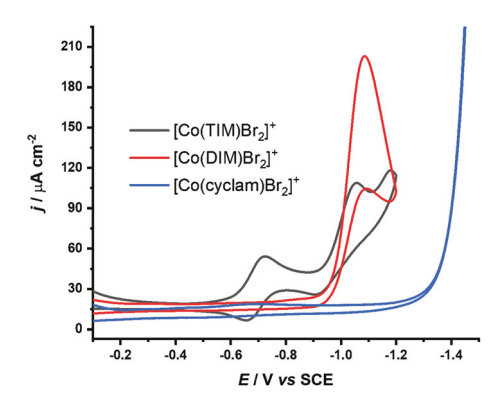


Fig. 5 Cyclic voltammograms of 0.5 mM $[Co(TIM)Br_2]^+$ (black), $[Co(DIM)Br_2]^+$ (red), and $[Co(cyclam)Br_2]^+$ (blue) in 0.1 M KBr, pH 6.0 with 10 mM NaNO₃. Working electrode glassy carbon, scan rate 5 mV s⁻¹.

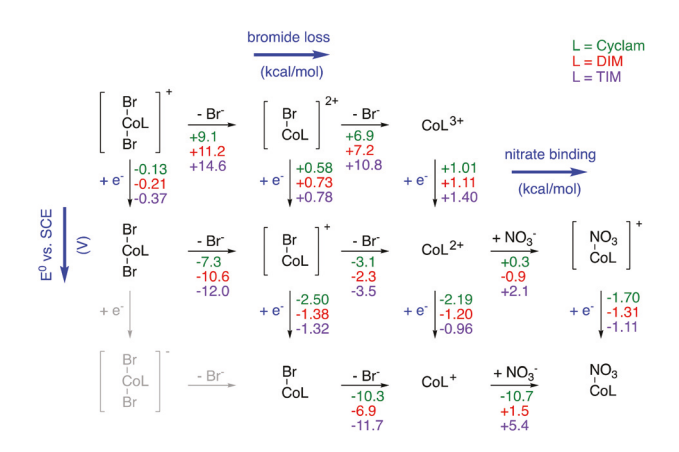


Fig. 6 Bromide dissociation and nitrate association with electron reduction scheme for Co-complexes generated by DFT calculations. The horizontal pathways correspond to the free energy of the reaction (ΔG) in kcal mol^{-1} and the vertical pathways correspond to the one-electron reduction, with the potential reported in V vs. SCE. Green values are for when L = cyclam, red values for L = DIM, and purple values for L = TIM. $[\text{Co(L)Br}_2]^-$ were not optimizable because bromide is readily dissociated from these "Co(i)" complexes.

Paper Dalton Transactions

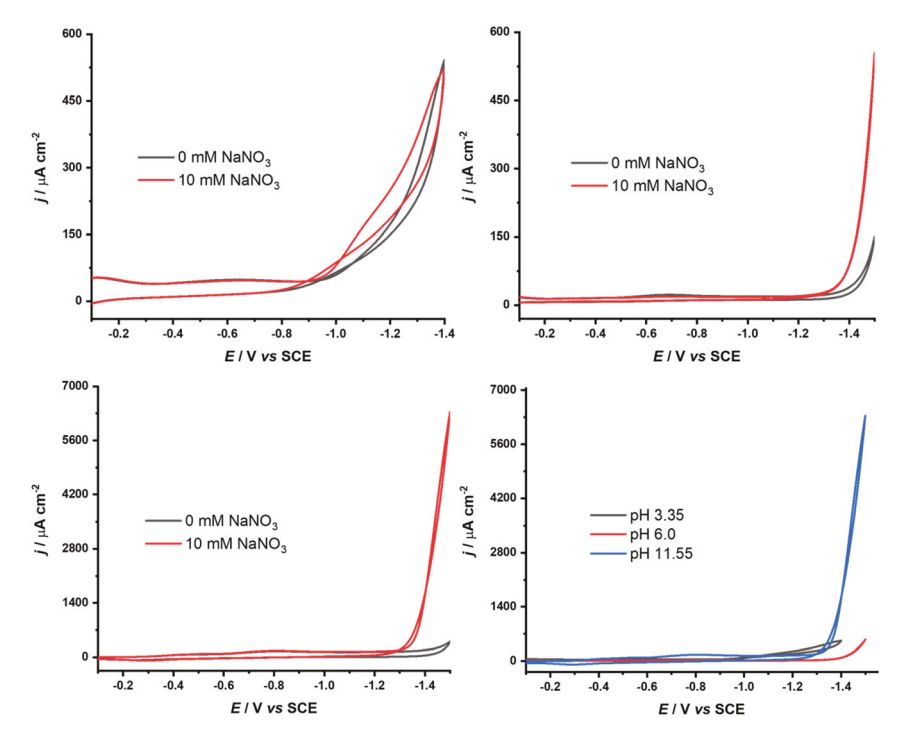


Fig. 7 Cyclic voltammograms of 0.5 mM [Co(cyclam)Br₂]⁺ (black) in 0.1 M KBr, with 10 mM NaNO₃ (red) at pH 3.35 (top left), 6.0 (top right) and 11.55 (bottom left). The activity at all three pH values is compared in the bottom right panel. Glassy carbon working electrode, scan rate 100 mV s⁻¹.

 $(TIM)Br_2]^+$ showed reversible one-electron waves with no evidence for catalytic activity. No significant differences in the UV-vis spectra of $[Co(cyclam)Br_2]^+$ following controlled potential electrolysis in the presence and absence of nitrate are observed, suggesting that the complex is stable under the electrocatalysis conditions (Fig. S7 and S8†).

Unlike $[Co(DIM)Br_2]^+$, which is active for electrocatalytic nitrate reduction in the pH range 4.4–10.4, but with the catalytic current independent of pH, the cyclic voltammograms of $[Co(cyclam)Br_2]^+$ show this complex has a greater catalytic current at higher pH, which decreases under acidic conditions (Fig. 7, bottom right). This may be caused by nitrate reduction competing with proton reduction at lower pH.³⁴ We mapped the possible interaction between $[Co(cyclam)]^{3+}$ and the solution at pH 3.35 and 11.55, with the results shown in the ESI (Fig. S9 and S10†). Among the possible interactions at pH 3.35, concerted proton–electron transfer (CPET) from $[Co(cyclam)Br]^+$ to $[Co(cyclam)BrH]^+$ was calculated to occur at $-1.16 \text{ V} \nu s$. SCE, which may account for the nitrate-independent peak (Fig. 7, top left).

Fig. 6 shows calculated square schemes for the Co complexes of interest. As can be seen, all $Co(\pi)L$ dibromo complexes (L = cyclam, DIM, and TIM) can be reduced to $Co(\pi)L$ dibromo complexes with potentials of -0.13 V, -0.21 V and -0.37 V νs . SCE, respectively. Two bromides can then be dissociated spontaneously for all three compounds. The diimine moieties of the DIM and TIM macrocycles can act as electron reservoirs. Thus, when $[Co(DIM)]^{3+}$ or $[Co(TIM)]^{3+}$ is reduced by two electrons, the first electron occupies a Co 3d orbital,

but the second electron occupies the ligand π^* orbital thereby avoiding forming the electron-rich Co(I) state. However, since $[\text{Co}(\text{cyclam})]^{2^+}$ does not have the conjugated π orbitals as electron reservoirs, the computed $\text{Co}(\Pi)/\text{Co}(I)$ reduction potential $(-2.19 \text{ V } \nu s. \text{ SCE})$ is noticeably more negative than the $\text{Co}(\Pi)L/\text{Co}(\Pi)L$ potential for $[\text{Co}(\text{DIM})]^{2^+}$ $(-1.20 \text{ V } \nu s. \text{ SCE})$ and $[\text{Co}(\text{TIM})]^{2^+}$ $(-0.96 \text{ V } \nu s. \text{ SCE})$. Overall, the $\text{Co}(\Pi)/\text{Co}(I)$ or $\text{Co}(\Pi)L/\text{Co}(I)$ reduction half potential is the most favorable for TIM followed by DIM and cyclam.

For the cyclam complex, the $Co(\pi)$ to $Co(\pi)$ reduction potential becomes less negative after nitrate binds to Co, even though the overall charge of the complex decreases (-1.70~V~vs. SCE for $[Co(cyclam)(NO_3)]^+$ compared with -2.19~V~vs. SCE for $[Co(cyclam)]^{2+}$). Nitrate bound to Co can serve as an electron acceptor, which is lacking in the cyclam ligand, promoting the reduction of the complex. This result agrees with cyclic voltammograms in Fig. 5 and 6, where nitrate reduction electrocatalysis is observed, despite the fact that the $[Co(cyclam)]^{2+/+}$ wave is not observed in the absence of substrate.

Binding competition in aqueous solution

The nitrate binding energies for [Co(DIM)]⁺ and [Co(TIM)]⁺ are 1.5 and 5.4 kcal mol⁻¹, respectively, while water binding energies are 2.3 and 3.6 kcal mol⁻¹ (Fig. 8). Note that negative binding energies suggest favorable binding, while positive energies indicate unfavorable binding. Thus, [Co(TIM)]⁺ thermodynamically favors the binding of water rather than

Dalton Transactions Paper

$$\begin{bmatrix} OH_2 \\ CoL \end{bmatrix}^+ \underbrace{ + H_2O}_{(+1.3)} & CoL^+ & \underbrace{ + NO_3^-}_{-10.7} & NO_3 \\ + 2.3 & & & + 1.5 \\ + OH^- & + 13.4 & & & + 20M \\ & & & & + 13.4 \\ & & & & + 16.9 \end{bmatrix}$$

$$CoL + \underbrace{ + NO_3^-}_{-10.7} & NO_3 \\ + 1.5 & & & \\ + 5.4 & & & \\ L = Cyclam \\ L = DIM \\ L = TIM$$

Fig. 8 Water, hydroxide and nitrate binding energies (ΔG) to $[Co-L]^+$ at pH = 0 in kcal mol^{-1} . $[Co(cvclam)]^+$ does not make a bond with water in its lowest energy state, instead a water molecule is stabilized at the position where hydrogen points at Co.

nitrate. From the calculated ΔG , we can approximate the equilibrium constant (K_{eq}) using the following equation:

$$\Delta G^{\circ} = -RT \ln K_{\text{eq}}. \tag{2}$$

As free energy increases, the K_{eq} and the relative concentration increase exponentially. Based on the calculated K_{eq} , water is about 24 times more likely to bind to [Co(TIM)]⁺ than nitrate, while nitrate is four times more likely to bind to [Co (DIM)]⁺ than water. This indicates that the substrate binding step is potentially rate-limiting for nitrate reduction by the [Co (TIM)]⁺ complex.

There is also the intermediate step of nitrate forming a hydrogen bonding interaction with the amino-protons of cyclam and DIM ligands before binding to Co. The electrostatic force between an oxygen atom of nitrate and an aminoproton of DIM and cyclam helps to introduce nitrate to a Co binding site, similar to the chelate effect. The hydrogen bonding also helps in preventing the nitrate detachment. Therefore, the TIM ligand, which does not have aminoprotons, would be the least favored for binding nitrate.

Nitrate reduction mechanisms

Table 2 shows free energies of activation for each pathway described in Fig. 2. Among the investigated mechanisms, the cyclam and DIM complexes prefer the amino-proton-assisted pathway while the TIM complex prefers the hydroxyl transfer pathway because of the absence of amino-protons on the TIM ligand. It is important to note that the free energy barriers for the amino-proton-assisted mechanism of the cyclam complex in Table 2 are calculated for nitrate binding to [Co(cyclam)]⁺ although the preferred pathway is nitrate binding to [Co (cyclam)²⁺ as discussed in the previous section. This was done to be consistent with the [Co(DIM)]⁺ and [Co(TIM)]⁺ preferred path-

Table 2 Free energy barriers for each mechanism for [Co(cyclam)]+, [Co(DIM)]⁺ and [Co(TIM)]⁺ complexes in kcal mol⁻¹

	Monodentate	Bidentate	5	Amino- proton-assisted
[Co(cyclam)]+	8.9	30.0	6.4	3.4
[Co(DIM)]+	19.5	22.0	13.3	13.3
[Co(TIM)]+	25.3	28.2	16.8	N/A

ways. The hydroxyl transfer and the amino-proton-assisted pathways for [Co(DIM)]+ share several intermediates leading to the rate determining step, but the amino-proton-assisted pathway has lower energy profile steps after the shared intermediates (see Fig. 10 and Fig. S11† for details). While only the most favorable pathway for each Co complex is presented here, the free energies for every other mechanism can be found in the ESI.†

Nitrate reduction with [Co(cyclam)]²⁺

The lowest energy pathway for nitrate reduction by [Co(cyclam)]²⁺ is shown in Fig. 9. As discussed previously, unlike DIM and TIM complexes, [Co(cyclam)]²⁺ (C2) is less likely to be reduced to [Co(cyclam)]⁺. However, after nitrate binds to C2 with the binding energy barrier of 8.5 kcal mol⁻¹, nitrate can serve as an electron acceptor, so the reduction process becomes more favorable by 0.49 eV. Also, it is important to note that from C3 to C4, nitrate becomes pyramidalized (average O-N-O angle changes from 120.0° to 116.2°), indicating that an electron has been transferred to the substrate rather than to cobalt. In structure C4, nitrate is also stabilized by hydrogen bonding between two amino-protons and two oxygen atoms (each hydrogen and oxygen distance being 1.854 Å and 1.871 Å). Once nitrate gains an extra electron from an external system, proton binding (C4 to C5) becomes a spontaneous process at any accessible pH ($\Delta G = -22.6 \text{ kcal mol}^{-1} \text{ at pH } 0, -3.6 \text{ kcal mol}^{-1} \text{ at pH}$ 14). Then, with assistance from the hydrogen bonding by an amino-proton, hydroxide can be dissociated from nitric acid with only a 3.4 kcal mol⁻¹ barrier to produce a water molecule. After the water molecule leaves, the [Co(cyclam)]²⁺ catalyst can be recovered by introducing another proton and an electron, which are spontaneous processes. Then, the calculated reaction barrier for the nitrate reduction cycle by [Co(cyclam)]³⁺, ignoring

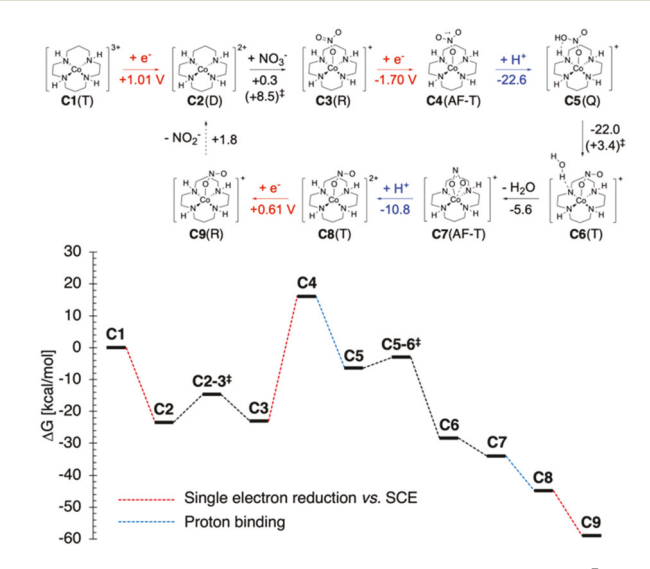


Fig. 9 Amino-proton-assisted mechanism with [Co(cyclam)]³⁺. The values are in kcal mol^{-1} for ΔG of the reaction and V vs. SCE for single electron reduction (converted to kcal mol⁻¹ in the diagram according to $\Delta G = -nFE^{\circ}$). The spin states are denoted as follows: doublet (D), triplet (T), antiferromagnetically-coupled triplet (AF-T), quartet (R), quintet (Q).

the electrochemical reduction steps, becomes 10.3 kcal mol⁻¹ measured from C9 to the nitrate binding step C2-3[‡] (note that [‡] labels the transition state structures).

Nitrate reduction with [Co(DIM)]²⁺

Paper

Unlike the cyclam complex, $[Co(DIM)]^{2+}$ (-1.20 V vs. SCE) is easier to reduce than the nitrate-bound complex [Co(DIM) NO_3]⁺ (-1.31 V vs. SCE) because of its redox-active ligand. Thus, nitrate can bind to cobalt after the complex is reduced to [Co(DIM)]⁺, which requires only 3.9 kcal mol⁻¹ (see Fig. 10).

For the nitrate reduction mechanism to proceed from D4 to **D6**, an electron and a proton need to be transferred to nitrate. As illustrated in Fig. 11, this can be done by four different pathways of proton-coupled electron transfer (PCET): an electron transfer followed by a proton transfer (ETPT) through a monodentate intermediate, ETPT through a bidentate intermediate, proton transfer followed by an electron transfer (PTET), and a concerted proton-electron transfer (CPET) in which proton transfer and intramolecular electron transfer occur simultaneously. The energies in Fig. 10 and 11 were calculated at pH 0, so note that the PTET barrier will increase as

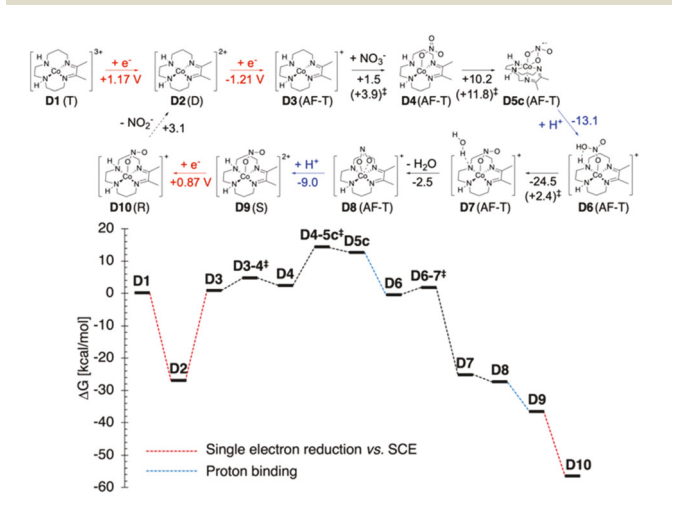


Fig. 10 Amino-proton-assisted mechanism for [Co(DIM)]³⁺. The values are in kcal mol⁻¹ for ΔG of the reaction and V vs. SCE for single electron reduction (converted to kcal mol⁻¹ in the diagram).

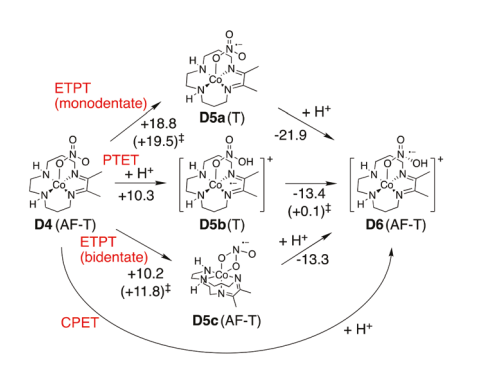


Fig. 11 Three proposed electron and proton transfer pathways for DIM complex. Free energies are reported in kcal mol⁻¹.

the pH increases (i.e., it increases by $9.5 \text{ kcal mol}^{-1}$ at pH 7). In a previous study, it was observed that the [Co(DIM)]⁺ nitrate reduction is pH independent. 15 Thus, neither PTET nor CPET can be the rate-determining step for the overall reaction. Therefore, ETPT through the bidentate mechanism is the most plausible pathway among the investigated mechanisms when considering all of the experimental evidence.

Once the nitric acid ligand is made (D6), hydroxide can leave and form a water molecule, acquiring the required proton from a DIM-amino group with a barrier of 2.4 kcal mol⁻¹. Finally, the catalyst is recovered after water leaves and another proton is introduced. Therefore, the overall rate-limiting step for the Co-DIM complex is the electron transfer step (D3 to D4-5[‡]) with a 13.3 kcal mol⁻¹ barrier. From the experimentally measured reaction rates at different temperatures, the Gibbs free energy of activation was determined to be 16.7 kcal mol⁻¹ at 298.15 K (see Fig. S17 in ESI†). Considering the accuracy of the DFT methodology and experimental measurement, they agree within the error range.

Nitrate reduction with [Co(TIM)]²⁺

The lowest energy pathway for nitrate reduction by [Co(TIM)]²⁺ is shown in Fig. 12. [Co(TIM)]²⁺ is reduced to [Co(TIM)]⁺ at an even more positive potential than [Co(cyclam)]2+ or [Co $(DIM)^{2+}$ because of the presence of another ligand π^* orbital that can act as an electron reservoir. After the reduction steps, nitrate binds to cobalt with a binding energy of 5.4 kcal mol⁻¹. Although the electronic energy of the T3-4[‡] transition state is higher than T4, as would be expected, it actually has a smaller free energy than T4 because the entropy at $T3-4^{\ddagger}$ is greater than the entropy at T4, most likely due to the change in the number of molecules (this step describes nitrate binding to [Co(TIM)]⁺ complex). From T4, a proton can be introduced to nitrate with an 11.6 kcal mol⁻¹ barrier to form a nitric acid complex (T5a). Alternatively, electron transfer from TIM to nitrate may occur with 11.3 kcal mol⁻¹ barrier to form bidentate complex T5b (Fig. 13). Again, the proton transfer step

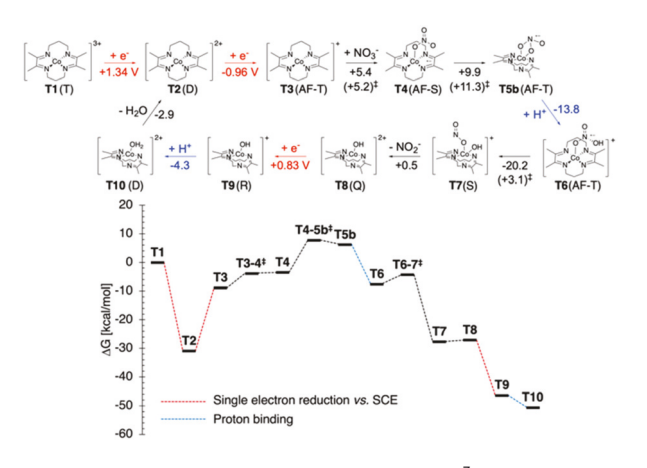


Fig. 12 Hydroxyl transfer mechanism for [Co(TIM)]³⁺. The values are in kcal mol^{-1} for ΔG of the reaction and V vs. SCE for single electron reduction (converted to kcal mol⁻¹ in the diagram).

Dalton Transactions Paper

Fig. 13 Two proposed electron and proton transfer pathways for TIM complex. Free energies are reported in kcal mol⁻¹.

from T4 to T5a is pH dependent, so the barrier becomes much higher under the actual experimental conditions (i.e. 21.1 kcal mol^{-1} at pH = 7). Thus, ETPT is again the more plausible pathway. After formation of the bidentate complex (T5b), a proton is introduced to make a nitric acid ligand (T6). Due to the excess electron on nitrogen and the flexibility of the TIM ligand, the N-OH bond of the nitric acid ligand can be easily cleaved with a 3.1 kcal mol⁻¹ barrier to transfer the OH group to the metal, thereby becoming an octahedral complex, T7. Then, nitrite can leave, and the catalyst can be recovered by introducing an electron and another proton to produce water. The barrier for [Co(TIM)]+ mediated nitrate reduction measured from T3 to T4-5 b^{\ddagger} is 16.8 kcal mol⁻¹.

Unlike mechanisms for cyclam and DIM complexes, the second proton introduction is pH dependent. At higher pH (>~7), this step becomes non-spontaneous, but it would still not exceed the activation barrier of the proposed mechanism in any reasonable pH range. Therefore, the reaction rate would not be affected by pH of the system.

Discussion

From the thermodynamics of the investigated mechanisms, [Co(TIM)]³⁺ was determined to not only favor binding water rather than nitrate, but also to have the highest activation barrier among the three complexes. The calculated 3.5 kcal mol⁻¹ difference between the DIM complex vs. the TIM complex may not be able to fully explain [Co(DIM)]⁺ being an active catalyst and [Co(TIM)]+ being inactive, but eqn (2) suggests the catalytic activity with DIM is ~368 times faster than with TIM. It is also important to note that the DFT thermodynamics, as well as the spin-state energetics, of the TIM complex are significantly more sensitive to the percent of exact exchange in a functional (see Fig. S16†). Depending on the functional chosen, the electronic energy barrier from the lowest energy intermediate to N-O cleaving for the [Co(TIM)]⁺ complex varies by as much as ~17 kcal mol⁻¹ (PBE vs. M06, Table S1†). Overall, the inactivity of the [Co(TIM)]³⁺ complex appears to be due to a combination of two factors: (1) poor substrate binding to the catalyst and (2) higher barrier for intramolecular electron transfer.

Summary and conclusions

The differences between [Co(cyclam)]³⁺, [Co(DIM)]³⁺ and [Co (TIM)]3+ were investigated electrochemically and computationally. The natural orbital analysis revealed the redox non-innocent nature of the DIM and TIM ligands, which resulted in occasional spin-state crossing throughout the modelled mechanisms. The presence of amino-protons in DIM and cyclam ligands enables a direct involvement of the aminoprotons in the mechanistic pathway for nitrate reduction, which was not considered previously. While [Co(cyclam)]³⁺ and [Co(DIM)]³⁺ reduce nitrate through the amino-proton-assisted mechanism, [Co(TIM)]3+ reduces nitrate through the hydroxyl transfer mechanism. Activation barriers for nitrate reduction with [Co(cyclam)]³⁺, [Co(DIM)]³⁺ and [Co(TIM)]³⁺ catalysts were calculated to be 10.3 kcal mol⁻¹, 13.3 kcal mol⁻¹ and 16.8 kcal mol⁻¹, respectively. The differences in the activation barriers are mainly due to substrate binding and the electron transfer process. We have also shown that there is a competition between water and nitrate to bind to the [Co(TIM)]⁺ complex, and as a result, nitrate is less likely to bind to [Co(TIM)]+ than its DIM and cyclam analogues.

Overall, [Co(DIM)]³⁺ was computationally shown to be the best electrocatalyst among the three Co complexes due to a combination of less negative reduction potentials, which is attributed to the redox non-innocent ligand acting as an electron reservoir, and an accessible reaction barrier, stimulated by intramolecular hydrogen bonding. Thus, in order to improve the nitrate reduction process with Co catalysts, testing of different substituents on the diimine side of the DIM-based structure is suggested.

Conflicts of interest

There are no conflicts to declare.

Acknowledgements

gratefully acknowledge funding from (CHE-2102442). EJ and HYK also acknowledge the support from the NSF grant CHE-1554855, as well as the services of the High-Performance Computing center at NCSU. SEB and JMS also acknowledge funding from the NSF (CHE-1566258). JPM acknowledges support from the NSF-REU program at NCSU (CHE-1659690).

References

- 1 V. Smil, Enriching the earth: Fritz Haber, Carl Bosch, and the transformation of world food production, 2000.
- 2 L. E. Apodaca, Nitrogen (Fixed) Ammonia, U.S. Geological Survey, 2019.
- 3 J. W. Erisman, M. A. Sutton, J. Galloway, Z. Klimont and W. Winiwarter, Nat. Geosci., 2008, 1, 636-639.

Paper Dalton Transactions

- 4 J. N. Galloway, A. M. Leach, A. Bleeker and J. W. Erisman, Philos. Trans. R. Soc., B, 2013, 368, 20130120.
- 5 S. Matassa, D. J. Batstone, T. Hulsen, J. Schnoor and W. Verstraete, Environ. Sci. Technol., 2015, 49, 5247-5254.
- 6 J. N. Galloway, A. R. Townsend, J. W. Erisman, M. Bekunda, Z. C. Cai, J. R. Freney, L. A. Martinelli, S. P. Seitzinger and M. A. Sutton, Science, 2008, 320, 889-892.
- 7 J. A. Camargo and A. Alonso, Environ. Int., 2006, 32, 831-849.
- 8 D. Fowler, M. Coyle, U. Skiba, M. A. Sutton, J. N. Cape, S. Reis, L. J. Sheppard, A. Jenkins, B. Grizzetti, J. N. Galloway, P. Vitousek, A. Leach, A. F. Bouwman, K. Butterbach-Bahl, F. Dentener, D. Stevenson, M. Amann and M. Voss, Philos. Trans. R. Soc., B, 2013, 368, 20130164.
- 9 S. H. Cheng and Y. O. Su, Inorg. Chem., 1994, 33, 5847-5854
- 10 Y. X. Guo, J. R. Stroka, B. Kandemir, C. E. Dickerson and K. L. Bren, J. Am. Chem. Soc., 2018, 140, 16888-16892.
- 11 X. N. Yang, D. L. Zhou and J. F. Rusling, J. Electroanal. Chem., 1997, 424, 1-3.
- 12 I. Taniguchi, N. Nakashima and K. Yasukouchi, J. Chem. Soc., Chem. Comm., 1986, 1814-1815.
- Taniguchi, N. Nakashima, K. Matsushita and K. Yasukouchi, J. Electroanal. Chem. Interfacial Electrochem., 1987, 224, 199-209.
- 14 H. L. Li, W. C. Anderson, J. O. Chambers and D. T. Hobbs, Inorg. Chem., 1989, 28, 863-868.
- 15 S. Xu, D. C. Ashley, H. Y. Kwon, G. R. Ware, C. H. Chen, Y. Losovyj, X. F. Gao, E. Jakubikova and J. M. Smith, Chem. Sci., 2018, 9, 4950-4958.
- 16 M. J. Frisch, G. W. Trucks, H. B. Schlegel, G. E. Scuseria, M. A. Robb, J. R. Cheeseman, G. Scalmani, V. Barone, G. A. Petersson, H. Nakatsuji, X. Li, M. Caricato, A. V. Marenich, J. Bloino, B. G. Janesko, R. Gomperts, B. Mennucci, H. P. Hratchian, J. V. Ortiz, A. F. Izmaylov, J. L. Sonnenberg, D. Williams-Young, F. Ding, F. Lipparini, F. Egidi, J. Goings, B. Peng, A. Petrone, T. Henderson, D. Ranasinghe, V. G. Zakrzewski, J. Gao, N. Rega, G. Zheng, W. Liang, M. Hada, M. Ehara, K. Toyota, R. Fukuda, J. Hasegawa, M. Ishida, T. Nakajima, Y. Honda, O. Kitao, H. Nakai, T. Vreven, K. Throssell, J. A. Montgomery Jr.,

- J. E. Peralta, F. Ogliaro, M. J. Bearpark, J. J. Heyd, E. N. Brothers, K. N. Kudin, V. N. Staroverov, T. A. Keith, R. Kobayashi, J. Normand, K. Raghavachari, A. P. Rendell, J. C. Burant, S. S. Iyengar, J. Tomasi, M. Cossi, M. Millam, M. Klene, C. Adamo, R. Cammi, J. W. Ochterski, R. L. Martin, K. Morokuma, O. Farkas, J. B. Foresman and D. J. Fox, Gaussian 16 Rev. A.03, 2016.
- 17 A. D. Becke, Phys. Rev. A, 1988, 38, 3098-3100.
- 18 C. T. Lee, W. T. Yang and R. G. Parr, Phys. Rev. B: Condens. Matter Mater. Phys., 1988, 37, 785-789.
- 19 A. D. Becke, I. Chem. Phys., 1993, 98, 5648-5652.
- 20 A. D. Becke, J. Chem. Phys., 1993, 98, 1372-1377.
- 21 S. Grimme, J. Comput. Chem., 2006, 27, 1787-1799.
- 22 A. V. Marenich, C. J. Cramer and D. G. Truhlar, J. Phys. Chem. B, 2009, 113, 6378-6396.
- 23 M. Dolg, U. Wedig, H. Stoll and H. Preuss, J. Chem. Phys., 1987, 86, 2123-2131.
- 24 J. M. L. Martin and A. Sundermann, J. Chem. Phys., 2001, 114, 3408-3420.
- 25 K. A. Peterson, D. Figgen, E. Goll, H. Stoll and M. Dolg, I. Chem. Phys., 2003, 119, 11113-11123.
- 26 M. M. Francl, W. J. Pietro, W. J. Hehre, J. S. Binkley, M. S. Gordon, D. J. Defrees and J. A. Pople, J. Chem. Phys., 1982, 77, 3654-3665.
- 27 P. C. Harihara and J. A. Pople, Theor. Chim. Acta, 1973, 28, 213-222.
- 28 R. Krishnan, J. S. Binkley, R. Seeger and J. A. Pople, J. Chem. Phys., 1980, 72, 650-654.
- 29 A. D. Mclean and G. S. Chandler, J. Chem. Phys., 1980, 72, 5639-5648.
- 30 C. J. Cramer, Essentials of Computational Chemistry: Theories and Models, John Wiley & Sons, 2nd edn, 2004.
- 31 C. P. Kelly, C. J. Cramer and D. G. Truhlar, J. Phys. Chem. B, 2006, 110, 16066-16081.
- 32 S. Xu, H. Y. Kwon, D. C. Ashley, C. H. Chen, E. Jakubikova and J. M. Smith, Inorg. Chem., 2019, 58, 9443-9451.
- 33 A. J. Cohen, P. Mori-Sanchez and W. T. Yang, Chem. Rev., 2012, 112, 289-320.
- 34 J. Schneider, H. Jia, J. T. Muckerman and E. Fujita, Chem. Soc. Rev., 2012, 41, 2036-2051.